Univerzita Karlova v Praze

Matematicko-fyzikální fakulta

BAKALÁŘSKÁ PRÁCE

Kristína Václavová

Experimentální studium ultrajemnozrnných slitin Ti pro využití v biomedicíně

Katedra fyziky materiálů

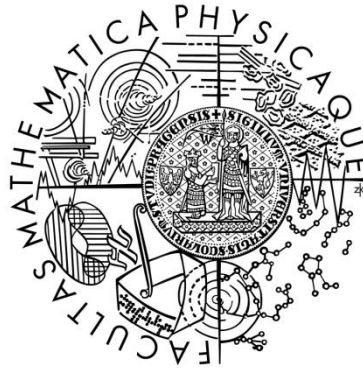Vedoucí bakalářské práce: RNDr. Josef Stráský

Studijní program: Fyzika

Studijní obor: Obecná fyzika

Praha 2013

Charles University in Prague

Faculty of Mathematics and Physics

BACHELOR THESIS

Kristína Václavová

Experimental characterization of ultrafine - grained Ti alloys for biomedical use

Department Of Physics of Materials

Supervisor of the bachelor thesis: RNDr. Josef Stráský

Study programme: Physics

Specialization: General Physics

Prague 2013

Acknowledgement

Název práce: Experimentální studium ultrajemnozrnných slitin Ti pro využití
v biomedicíně

Autor: Kristína Václavová

Katedra / Ústav: Katedra fyziky materiálů

Vedoucí bakalářské práce: RNDr. Josef Stráský, Katedra fyziky materiálů

Abstrakt: V předložené práci je studován vývoj mikrostruktury slitiny Ti-6Al-7Nb připravené pomocí torze za vysokého tlaku (high pressure torsion - HPT) a protlačováním pravoúhlým kanálem (equal channel angular pressing- ECAP). Experimentální studium probíhalo pomocí skenovací elektronové mikroskopie, měřením mikrotvrdosti a elektrického odporu. Elektronová mikroskopie prokázala bimodální strukturu slitiny a dále silně deformovanou strukturu po HPT. Mikrotvrdost se zvyšuje se vzrůstajícím počtem otáček během deformace pomocí HPT. Pomocí difrakce zpětně odražených elektronů se prokázalo, že misorientace zrn není náhodná. Změny elektrického odporu v slitině připravené metodou ECAP během lineárního ohřevu a chlazení prokázaly ireverzibilní proces uvnitř vzorku.

Klíčová slova: ultrajemnozrnné materiály, slitiny titanu, skenovací elektronová mikroskopie, měření elektrického odporu

Title: Experimental characterization of ultrafine-grained Ti alloys for biomedical use

Author: Kristína Václavová

Department / Institute: Department of Physics of Materials

Supervisor of the bachelor thesis: RNDr. Josef Stráský, Department of Physics of Materials

Abstract: In the present work the microstructure evolution of Ti-6Al-7Nb alloy prepared by high pressure torsion (HPT) and equal channel angular pressing (ECAP) was studied by scanning electron microscopy, microhardness measurements and electrical resistance measurements. Electron microscopy showed a bimodal structure of the alloy and deformed structure after HPT. Microhardness increased with the increasing number of turns of high pressure torsion. Electron back-scattered diffraction figured out that the grain misorientations are not random. Changes in the electrical resistance of the alloy prepared by ECAP showed irreversible process after heating above 450°C.

Keywords: ultra-fine grained materials, Ti-based alloys, scanning electron microscopy, electrical resistivity

Contents

1. Introduction

1.1 Titanium

Titanium was discovered in 1791 in minerals by a British mineralogist and chemist, William Gregor. The first commercial metal was produced by the Titanium Metals Company of America. Titanium is not really a rare substance. This material is the fourth most abundant structural metal in the Earth's crust inside which the titanium´s concentration is about 0.6%. [1].

Characteristic properties of titanium are extreme corrosion resistance, relatively high strength, sufficient biocompatibility, low density and moderate elastic modulus [2]. For dental and orthopedic applications can be used commercially pure titanium (CP Ti) primarily due to its excellent biocompatibility. On the other hand, limited strength refuses using CP titanium as a material for orthopedic endoprostheses. For that reason, the most widely used is still Ti-6Al-4V alloy, one of the oldest Ti alloys. However, the aforementioned alloy has some limitations. Special problem is the presence of vanadium that is known to be toxic element. For avoiding this harmful effect to organism a new Ti alloy was developed, Ti-6Al-7Nb which instead of vanadium contains niobium [3, 4]. In spite of different composition of these two materials, Ti-6Al-7Nb alloy has similar mechanical properties and undergoes similar phase transformations like Ti-6Al-4V.

Titanium is a polymorphic material. Above so-called beta-transus temperature, the material consists purely of β phase with body-centered cubic (bcc) crystallographic structure. Upon cooling, material transforms to α phase with hexagonal close-packed (hcp) structure. Investigated Ti-6Al-7Nb alloy belongs to α+β alloys meaning that material includes both α and β phases at room temperature [5].

1.2 Ultrafine-grained materials

A very small grain sizes (in the submicrometer and the nanometer range), homogeneous and equiaxed microstructure are characteristic for the ultra-fine grained (UFG) materials. This type of materials has excellent mechanical properties, such as strength, hardness, fatigue resistance or strength-to-weight ratio. Some UFG materials are superplastic thanks to enhanced grain boundary sliding. The reduction of grain size in polycrystalline materials cause changes in mechanical and physical properties. For example, the strength of the polycrystalline material changes with the grain size d according to the Hall-Petch equation [6, 7]

$$\sigma_y = \sigma_0 + k_y d^{-1/2} \tag{1.1}$$

where σ_y is the yield stress of the material, σ_0 represents the friction stress and k_y is a material constant.

Presently two types of producing UFG materials are known which are reported as the "bottom-up" and the "top-down" approach.

The "bottom-up" approach is to make ultra-fine powders and to consolidate them. The methods which applying "bottom-up" technique are, for example, the electrodeposition [8], inert gas condensation [9], ball-milling [10] or cryo-milling [11]. However, these types of techniques have disadvantages, which are manifested in some degree of residual porosity in the material and potential contamination.

The inverse process to "bottom-up" approach is a "top-down" technique. Rolling, forging and extrusion are between well-known conventional methods of grain size reduction. Today the most common procedures for the preparation UFG matters are severe plastic deformation (SPD) processes.

The most often used SPD processes are equal-channel angular pressing (ECAP) [12], high pressure torsion [13, 14], accumulative roll-bonding (ARB) [15], friction stir processing (FSP) [16, 17], repetitive corrugation and straightening (RCS) [18, 19], twist extrusion [20, 21]. The first two methods will be described in the following section.

1.3 Equal-channel angular pressing

Equal-channel angular pressing (ECAP), which is also known as equal-channel angular extrusion (ECAE), has some advantages:

- It is a relatively simple method.
- It can be used successfully for a wide range of metallic materials with different crystallographic structure, precipitation hardened materials, intermetallics, metal matrix composites, etc.
- ECAP allows repeated use of the stock with the same geometric shape without major modifications between cycles.
- Materials prepared by this method are mostly homogeneous and the whole process takes place as readily achievable under normal pressures and strain rates.
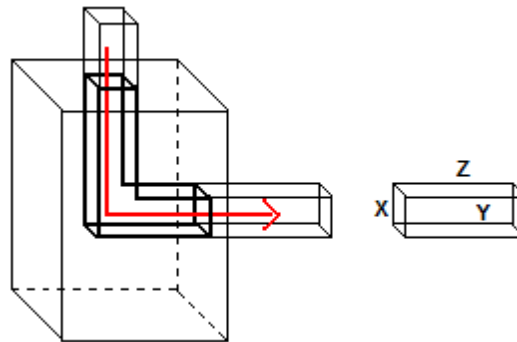
Fig. 1.1 Schematic representation of a typical die for ECAP

The basic idea of the ECAP process is that the prepared sample is pressed through a special die (Fig 1.1). The ECAP die is composed of two channels of the same cross-section, which together form an angle Φ. The most frequently used dies use the angle of 90°. There are also more complex dies where the channels do not meet at a right angle. Angle Ψ characterizes the "bend" of the channel that may not be sharp, but rounded as demonstrated on Fig 1.2.
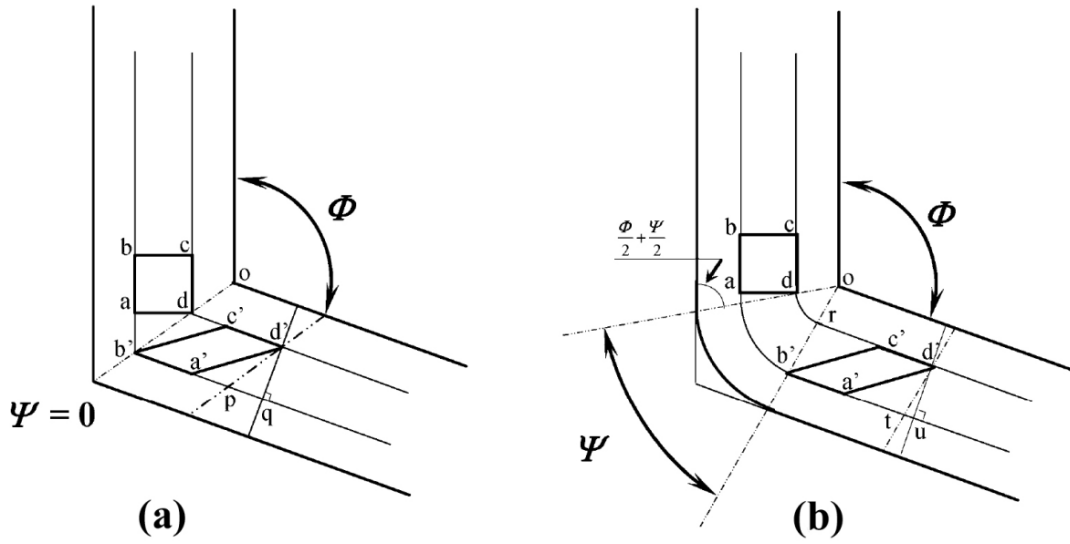
Fig. 1.2 Shear deformation during ECAP: a) $\Psi = 0$ or b) $\Psi \neq 0$ [22]

Material is deformed by simple shear during angular pressing. Deformation ε_{VM} stored in the material after a single pass through the die depends on its geometry and can be determined from the relationship [22]

$$\varepsilon_{VM} = \frac{1}{3}[2\cot\frac{\Phi}{2}+\frac{\Psi}{2} + \Psi\csc(\frac{\Phi}{2}+\frac{\Psi}{2})]$$ (1.2)

Due to the same geometric shape of both channels the extrusion process can be repeated, thereby increasing the total embedded deformation. Total deformation after N repetitions can be expressed as:

$$\varepsilon_N = N\varepsilon_{VM}$$ (1.3)

1.4 High pressure torsion

The second most common SPD procedure is high pressure torsion (HPT). High pressure torsion procedure is schematically illustrated in Fig 1.3. The disc-shaped sample is positioned between two anvils which compress the sample with high pressure (several GPa). Then one of the anvils starts rotating (depending on the particular configuration of the machine). The deformation is usually performed at room temperature. However, the anvils might be heated and deformation may be performed at elevated temperatures. There are several models to express the total equivalent strain induced by HPT.
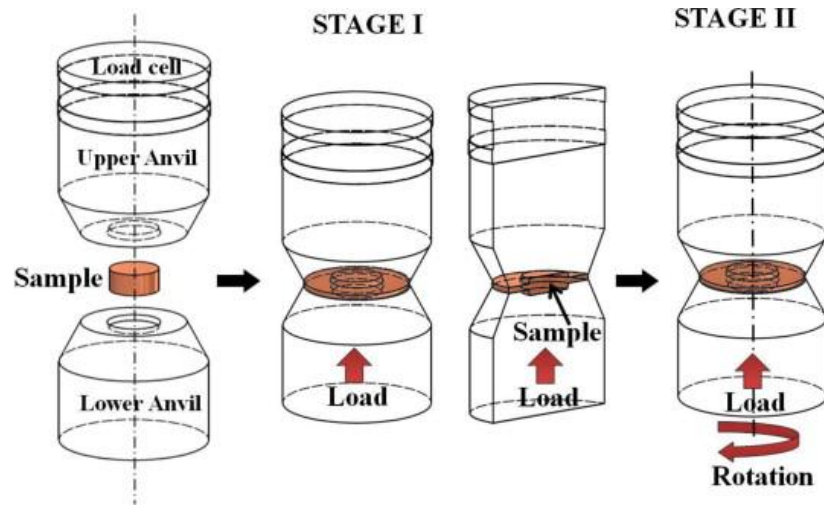
Fig. 1.3 Schematic representation of HPT [23]

Following model takes into account sample thickness reduction [24]:

$$\varepsilon_{VM} = \ln\left(\frac{2\pi Nrh_0}{h^2}\right) \tag{1.4}$$

The advantages of HPT compared to the ECAP method is higher achievable equivalent strain leading to materials with smaller grain size than with ECAP process. Nevertheless, the disadvantages are small size of the samples and non-homogeneous deformation. This inhomogeneous strain causes a radially inhomogeneous microstructure of specimen and finally inhomogeneous material properties. After 5 or 8 rotations (depending on material) almost homogenous deformation distribution was noticed by several authors [25, 26] who measured microhardness profiles through the sample cross-section. Otherwise, this disadvantage of inhomogeneity could be eliminated with using ring samples [27].

2. Aims of the thesis

The ultimate goal of the research in the present work is the characterization of the microstructure and physical properties of Ti-6Al-7Nb alloy after HPT and ECAP. This present work focuses in particular on:

- Dependence of the microhardness of the sample on distance from center of the sample and after different number of HPT revolutions
- EBSD analysis of misorientations of alpha lamellae in alpha + beta alloy Ti-6Al-7Nb
- Analysis of resistivity evolution during repetitive heating and cooling in Ti-6Al-7Nb alloy after ECAP

3. Experimental material

The received material was a rod with the diameter of 22 mm in as-rolled condition.

In order to create homogeneous UFG structure, it is effective to enhance the fraction of thin-plate β-transformed structure, the fragmentation of which occurs easier in the process of SPD. It is necessary to preserve the fraction of the primary α phase (usually about 20%) in the microstructure in order to inhibit growth of β grains and provide sufficient ductility due to increase of the free path length of dislocations in coarser grains [28].

The process of preparing Ti-6Al-7Nb alloy with bi-modal structure consists of 4 steps: homogenization in the β phase field, deformation in the α+β phase field, recrystallization in the α+β phase field and the final ageing and/or stress relieving treatment [29].

In the first step, cooling rate from beta region determines the width of the α lamellae. These α lamellae are deformed plastically in the second step. In the recrystallization annealing step, the temperature and time of annealing determine the volume fraction of the recrystallized primary α (α_P) located at the "triple-points" of the recrystallized β grains. α_P volume fraction and the α_P size specifies principal microstructural feature of the duplex structure.

3.1 Thermal treatment before HPT and ECAP

3.1.1 Thermal treatment before HPT

Thermal treatment (TT) was applied before HPT and it consists of recrystallization annealing at 985 °C (Beta transus temperature of Ti-6Al-7Nb alloy is around 1010 °C) for one hour followed by quenching to room temperature and an annealing at 700 °C for 4 hours. The microstructure after TT is showed in Fig. 3.1 [30]. In the Ti-6Al-7Nb alloy after the thermal treatment the α phase´s volume fraction was 18 % and the average size of α grains was 5.3 μm.
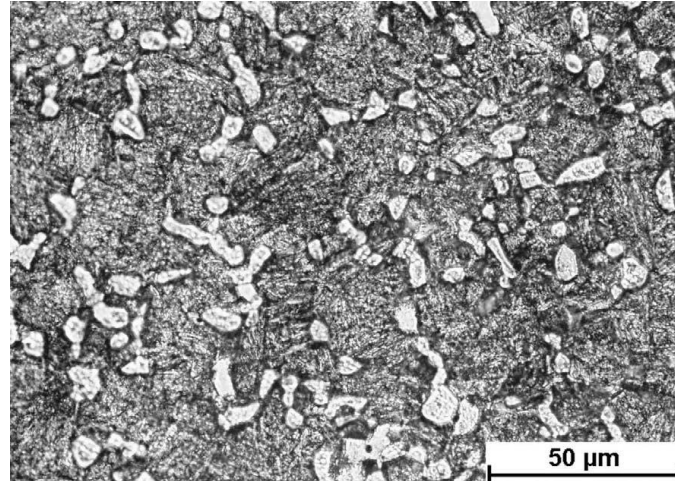
Fig. 3.1 Light microscopy image of Ti-6Al-7Nb after thermal treatment

3.1.2 Deformation by HPT

Samples with 20 mm diameter and a 2 mm thickness were obtained by electric discharge wire cutting. The sample was polished before applying high pressure torsion. The specimen was positioned between the anvils during HPT method. In our case the furrow was 0.8 mm high and the sample was subjected to compressive pressure of 6 GPa. Simultaneously, the lower anvil was rotated by the speed of 0.5 rpm. Deformation was accomplished at room temperature. The series of specimens which was prepared for testing was after ¼, ½, 1, 3, 5 and 15 turns [30].

3.1.3 Thermal treatment before ECAP

Before ECAP the material was thermally treated at USATU Ufa, Russia by the partners of this research. This thermal treatment is schematically illustrated in Fig. 3.2.

In the first step, annealing at temperature just below β transus was applied followed by water quenching. Bi-modal microstructure was reached after consequent annealing and cooling as described above.
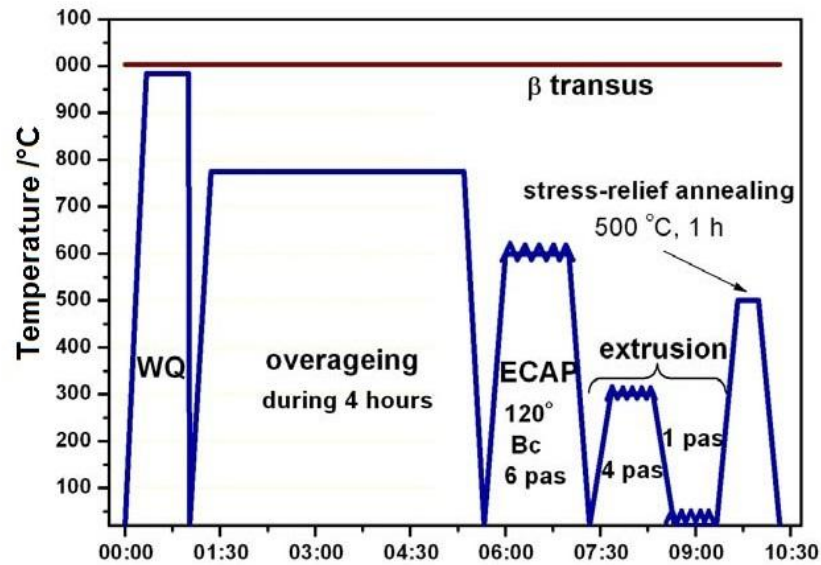
Fig. 3.2 Schematic illustration of thermal treatment before ECAP [31]

3.1.4 Deformation by ECAP

The ECAP die with angles $\Phi = 120°$ and $\Psi = 0°$ was utilized. The pressing was repeated six times. The resulting deformation according to the formulas (1.2) and (1.3) is: $\varepsilon_N = 4$. ECAP was followed by extrusion with extrusion ratio $ER = 4$. Stress relief annealed was performed at 500°C for 1 h.

3.2 Sample preparation

3.2.1 Microhardness and light microscopy

The samples after HPT are discs of approximate thickness of 0.8 mm and diameter 20 mm. However, due to leaking of the material during HPT, the disc is surrounded by the leaked material that is of no use (Fig. 3.3). This leaked material was removed by grinding on 80 grit (European FEPA grading) SiC grinding paper to get 20 mm diameter samples. For the purpose of microhardness measurements, samples have to properly polish. One of the reasons is that automatic microhardness tester is unable to identify indents in presence of contaminations and scratches.

The samples were mounted first. Electrically conductive mounting material (PolyFast by Struers) was used to allow also SEM observations. The specimens were mechanically grinded to eliminate any impurity on the surface. Approximately 0.3 mm of thickness was removed. Secondly, specimens were ground applying 500, 800, 1200, 2400 grit SiC papers. Afterward, the samples were polished on polishing disc with polishing suspension (diamond paste) of grade (with particle size of) 3 μm. Final polishing was done by active oxide polishing suspension (OP-S supplied by Struers).

Fig. 3.3 Sample surrounded by the leaked material

3.2.2 SEM observations

For some SEM observations we also used unmounted specimens. Thin specimens were glued to cylindrical Al pad for polishing. Treating of specimens was similar to treating for microhardness testing, but for grinding were used 500, 800, 1200, 2400 and 4000 grit SiC papers. Finally, a vibratory polisher was use employing 0.3 μm and 0.05 μm aqueous alumina (Al_2O_3) suspensions and colloidal silica.

3.2.3 Resistivity measurement

For resistivity measurements, we prepared samples from rod made of Ti-6Al-7Nb alloy after ECAP. Approximately 1 mm thick, 10 mm wide and 15 mm long plates were cut from the rod using Struers Accutom-50. The final shape of samples is showed on the Fig. 3.4 what was achieved with a diamond wafering blade with 5 mm width. Each specimen was ground applying 320, 500, 800, 1200 grit SiC papers. The final width of samples was close to 0.7 mm. Four contacts made from commercially pure titanium wire were placed on the sample. The titanium wire was used to minimize the contact resistance between the sample and the probe.
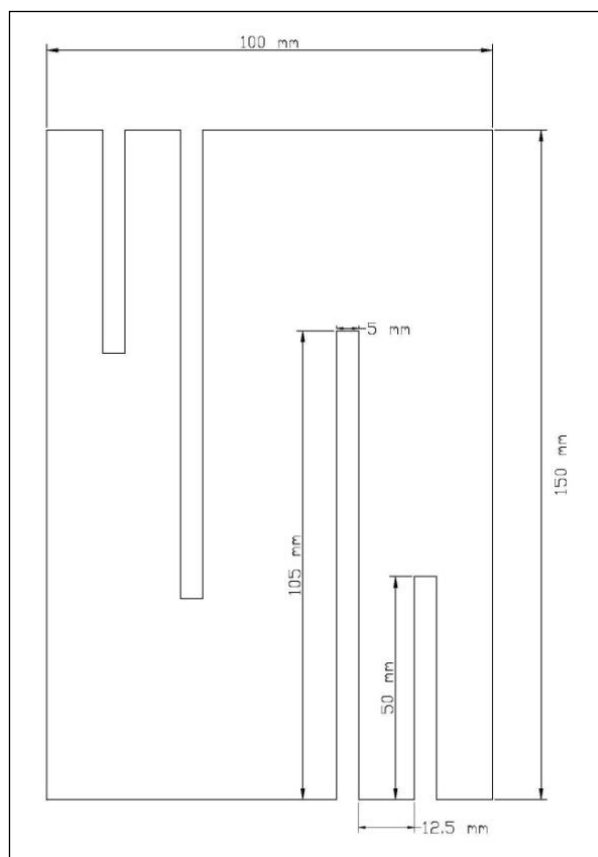

Fig. 3.4 Shape of the samples for resistivity measurement

4. Experimental methods

4.1 Microhardness measurement

The microhardness of specimens was measured by Vickers method on automatic microhardness tester Qness Q10a. In the Vickers method, the diamond indenter has the form of a square-based pyramid with the top angle between sides equal to 136°. Firstly, the indenter is pressed into the surface of the specimen with a specified force for duration of 10 s. An indentation left in the sample a surface area A, which can be expressed by the formula

$$A = \frac{d^2}{2\sin(\frac{136°}{2})},$$
(4.1)

where d means the average length of the diagonal of the indentation left by the indenter in millimeters. The equation (4.1) can be approximated to give

$$A \approx \frac{d^2}{1.8544}.$$
(4.2)

The resulting microhardness value (HV number) is determined by the ratio F/A

$$HV = \frac{F}{A} \approx \frac{1.854F}{d^2},$$
(4.3)

where F is the applied force.

More than 1000 indents were applied on disc specimen in a square grid with higher density near the sample center. Higher density of indents near specimen center was used to obtain sufficient amount of measurements to investigate the dependence of microhardness on equivalent strain (i.e. the distance from the center). The scheme of distribution of indents is illustrated in Fig. 4.1. This scheme was prepared by AutoCAD and the coordinates of points was exported to *.csv file that can be used for fully automated microhardness measurement.
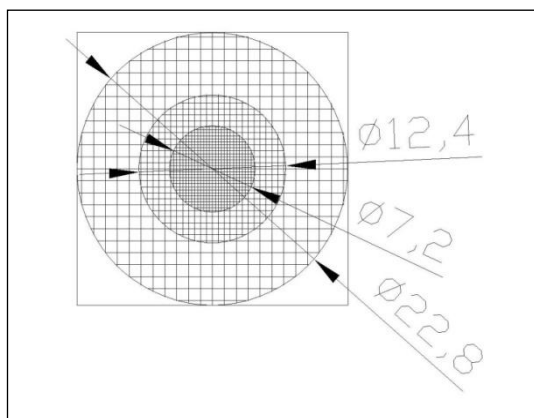
Fig. 4.1. Schematic illustration of distribution of indents

4.2 Scanning electron microscopy (SEM)

Direct observations of the microstructure of the Ti-6Al-7Nb alloy were accomplished by scanning electron microscope FEI Quanta 200F. The source of electrons in the microscope is a field emission gun (FEG).

The electrons which were emitted from the cathode (FEG) are accelerated. This primary beam hits the sample and the electrons interact with the atoms of the material. This interaction is reflected in the formation of different signals which are detected by microscope. The signals give information about the topology or composition of the specimen.

The first type of signals that can be detected are back-scattered electrons (BSE). BSE are utilized to investigate the chemical contrast of the sample. This contrast is given by chemical composition – so-called Z-contrast. The Z-contrast is caused by the different atomic number of elements. Heavy elements with higher atomic number scatter the electrons more strongly than light elements, so the number of back-scattered electrons is higher. For that reason, heavier elements appear brighter in the BSE image.

BSE can also be used in electron back-scatter diffraction (EBSD) visualising to find out various crystallographic parameters.

Other signals which can be detected by SEM are secondary electrons (SE). After inelastic scattering of the primary beam at the sample these electrons are emitted from the electron shell. Only secondary electrons, which are ejected near the surface, can be detected. The topology of the surface indicates the amount of emitted secondary electrons. [32]

14

When the electron interacts with the inner shell of specimen atom it might eject other electron from its orbital. Then the inner shell vacancy can be filled by an electron from an outer, higher energy shell. The energy difference between the two shells can be released in two ways. In the Auger process, the energy is used to eject another outer shell electron. In the characteristic X-ray process, the excess energy is released in the form of a characteristic X-ray radiation [33]. Energy dispersive X-ray spectroscopy (EDX) is used for the chemical characterization of the sample. Characterization of individual elements is based on the fact that each element in atomic structure has a unique set of peaks in its X-ray spectrum [34].

Electron back-scattered diffraction (EBSD) is a method which provides information about the microstructure of material and grains orientation. For example, texture, grain size, misorientation of individual grains and many other features may be acquired from EBSD results. The EBSD measurement is based on the inelastic electron scattering. This type of scattering causes so-called Kikuchi lines. Because each Kikuchi line is associated with Bragg diffraction, Miller indices can be assigned to each Kikuchi line and according to the shape of Kikuchi lines, the crystallographic orientation of the material in given point can be evaluated. Crystallographic orientation might be associated with specific colour according to the orientation triangle and so-called inverse pole figure map can be created.

4.3 Resistivity measurement

By studying the dependence of electrical resistance on temperature we can obtain information about microstructure and phase composition of studied material [35].

Resistivity of specimens was measured by four-point method. This measurement is based on the fact that the two outer contacts bring current to the sample from an external DC power source and the internal contacts are connected to a suitable voltmeter which measures the potential difference.

5. Result and discussion

5.1 Microhardness of material after HPT

The samples after measurement (i.e. after using more than 1000 indents) are illustrated on Fig. 5.1.
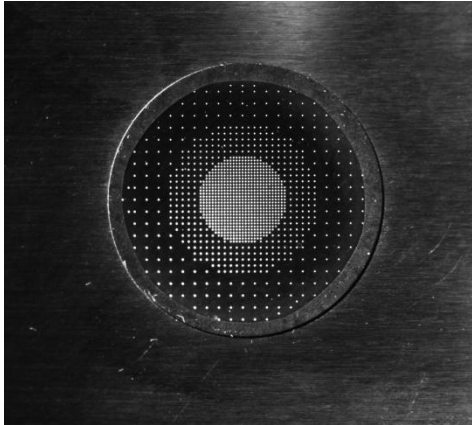

Fig 5.1 Sample after microhardness measurement

For the measurement, the load of 0.5 kg and indentation time 10 s for each indent were used. The observations were carried out for samples: as-rolled (as-received sample without HPT deformation), as-pressed (only pressed without rotation), samples after ¼, ½, 1, 3, 5, 15 turns.

Fig. 5.2 shows the microhardness line profiles, i.e. dependence of the microhardness on the distance from the center of the sample. Each displayed point is computed as the average of more than 100 indents measured around given distance from the center (i.e. point at $r = 1$ mm is average of indents in distance $0.5 - 1.5$ mm from the center). Error bars show standard deviations. The error bars are surprisingly large and do not correspond to the inherited error of the measurement that is lower by more than one order of the magnitude. Low precision of measured data is therefore given by the heterogeneity of the material microstructure and/or possible local inhomogeneity in the degree of deformation. The diagonal of each indent is approximately 50 μm.
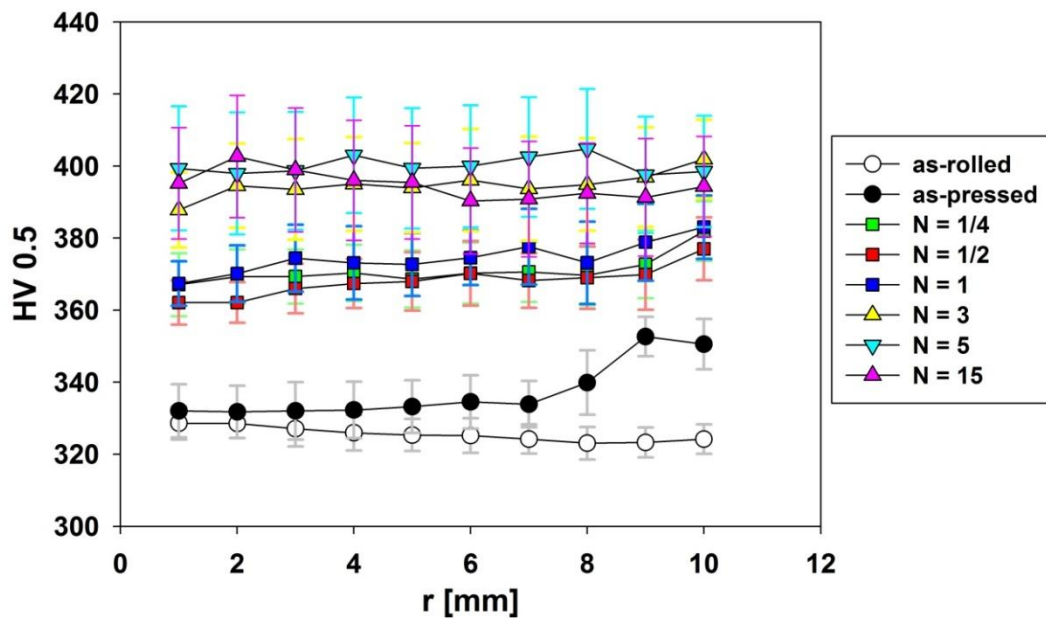
Fig. 5.2 Dependence of the microhardness on number of HPT turns and the distance from the center of the specimen

The heterogeneity of the material may imply that one indent is in the alpha lamellae (alpha + beta region) and another in the alpha grains. It is well known alpha grains are much softer than the alpha + beta region. In another case, it may occur that the indent is precisely on the boundary of individual grain or on the boundary grain and lamellae. Results of microhardness test show that specimen even after ¼ of turns of HPT is more hardened than without any HPT deformation. Moreover, results of measurements indicate that there is a significant increase of microhardness with increasing number of turns until N = 3. On the other hand, no significant increase of microhardness with distance from the center of the specimen is observed. Some increase is seen only for N = ¼ and N = ½. At higher deformations, the microhardness is homogenous over the whole specimen, which is a favorable result for any potential application. Finally, an increase in microhardness at the edge of as-pressed (N = 0) specimen is due to material outflow from underneath the pressing anvils, which effectively causes plastic deformation accompanied with microhardness increase. Similar effect was also observed in other materials [36].

5.2 SEM observations of material after HPT

Scanning electron microscopy was used for studying microstructure of the sample deformed by high pressure torsion after various numbers of turns. Microstructure of as-pressed specimen (i.e. specimen compressed between the anvils by a pressure of 6 GPa, but without any rotation) and specimen after 5 turns was observed by SEM using back-scattered electrons.

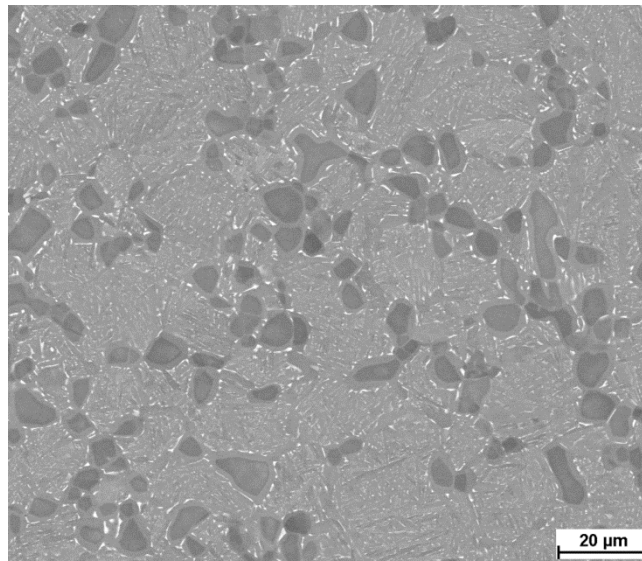### 5.2.1 As-pressed (N = 0) material

Fig. 5.3 As-pressed sample (N=0), an overview SEM image

In the Fig. 5.3 is showed the microstructure of as-pressed Ti-6Al-7Nb alloy after HPT. The bigger and darker grains are primary alpha grains; in addition, on the image are visible alpha + beta lamellae and small beta particles. Fig. 5.4 shows the more detailed micrograph of as-pressed material. The contrast between darker and lighter areas is given by chemical composition – so-called Z-contrast. Darker areas include elements with lower atomic number and lighter areas with higher atomic number. Our alloy Ti-6Al-7Nb contains aluminum as alpha-stabilizing element and niobium as beta-stabilizing element. Alpha grains contain more alpha-stabilizer, aluminum whose atomic number is much lower than that of titanium and niobium and therefore they appear darker. Beta phase contain more beta-stabilizer, niobium with atomic number 41 and therefore small beta particles around primary alpha grains and between alpha lamellae appear white.
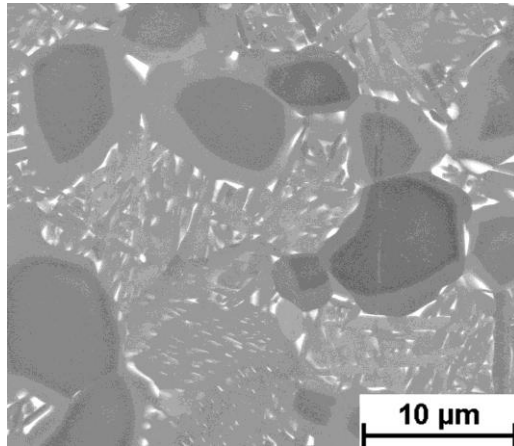
18

Fig. 5.4 As-pressed sample (N=0),
detail SEM image
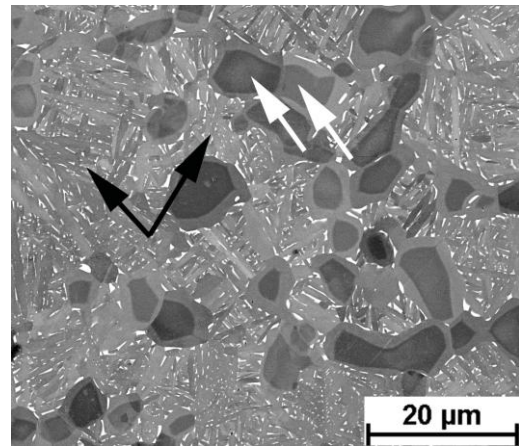(back-scattered electrons, Z-contrast)

Fig. 5.5 As-pressed sample (N=0), an
overview SEM image. Arrows point to
the areas with different channeling
contrast

Furthermore, distinct darker and lighter areas can be distinguished within single primary alpha grain. The difference between the edge and the middle is caused by different content of aluminum and/or niobium. The center of alpha grains is darker because it includes more aluminum and/or less niobium and is therefore more alpha-stabilized. Lighter areas contain comparatively more niobium and/or less aluminum.

Fig. 5.5 is also a SEM image in which are visible two types of contrasts. The first type is above discussed Z-contrast that is noticeable in each alpha grain. The second type is channeling contrast - grains with different orientation may have different contrast due to different absorption of back-scattered electrons. White arrows point to the two adjacent alpha grains with different shades, which are caused by their different orientation only. Furthermore, channeling contrast shows that lamellae in one area have the same crystallographic orientation, but in different areas the orientation is different. This is illustrated by black arrows. Each such group of lamellae evolves from a single beta grain since lamellae are created during cooling from beta region [37]. Crystallographic orientation of alpha lamellae will be discussed below in detail employing EBSD analysis.

The chemical composition was measured by energy dispersive X-ray scattering (EDX) and is shown in the Table 5.1 below. First, the average chemical composition was evaluated by X-ray signal acquisition over sufficiently large area so that composition is averaged over all microstructural features. The result of the

chemical composition shows that the theoretical composition (Ti – basic, Al – 6.17 %, Nb – 7.05 %, Fe – 0.14%, O – 0.17 %, C – 0.01 %, N – 0.03 %, Ti-balance) does not correspond quantitatively to the EDX measurements that suggest that the Ti-6Al-7Nb alloy contains more aluminum and niobium. However, it must be noticed that EDX measurements have qualitative character only and should be used mainly for direct comparison. Second, the chemical composition was locally measured near the edge and in the interior of alpha grains and in beta particles. Presented results are averages from three different points, but those data should be taken as qualitative only especially for beta phase, because the beta particle size is comparable to the interaction volume of the electron beam.

wt. %	Average	Alpha - edge	Alpha - int.	Beta
Ti	83.0	83.2	85.1	75.7
Al	8.6	8.5	10.0	6.4
Nb	8.5	8.3	4.9	16.4
Fe	0.0	0.0	0.0	1.4

Table 5.1 Chemical composition of different microstructural features, measured by EDX.

As shown in Table 5.1, the composition in the edge of alpha grains is similar to the average composition; however, the composition inside the alpha grains shows increased content of alpha stabilizing aluminum. On the other hand, beta regions are niobium enriched, which is in accordance with SEM observations using BSE. From the table it can be seen that the beta phase also contains iron. This element (Fe) is impurity in initial material which concentrates in the beta particles during annealing because iron is a strong beta-stabilizer.

5.2.2 Material after HPT (5 turns)

Material after deformation by high pressure torsion was examined by SEM in three different places. The scheme of the observation is showed in Fig. 5.6.

Fig. 5.7 shows the microstructure of the center specimen after 5 turns. Alpha grains are still well distinguishable and they are mostly round – similarly to the original material. However, each grain is obviously strongly deformed. Alpha grains have uneven shade due to deformation and contrast difference between the edge and the grain interior is not recognizable. Alpha + beta phase lamellar areas remain

straight in some zones – similarly to the as-pressed material, but in other areas they are already heavily deformed.
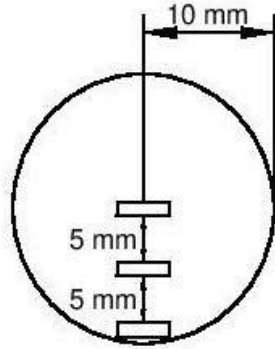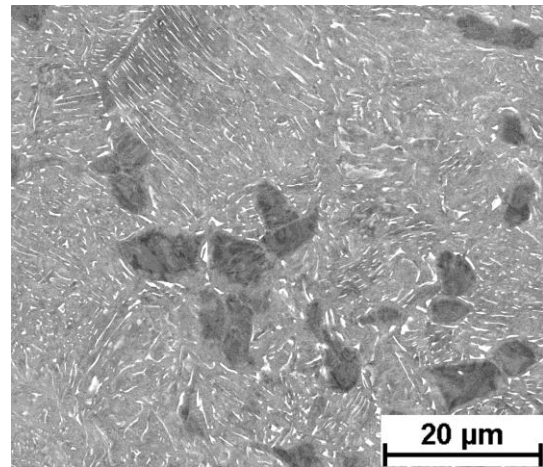

Fig. 5.6 Scheme of SEM observations

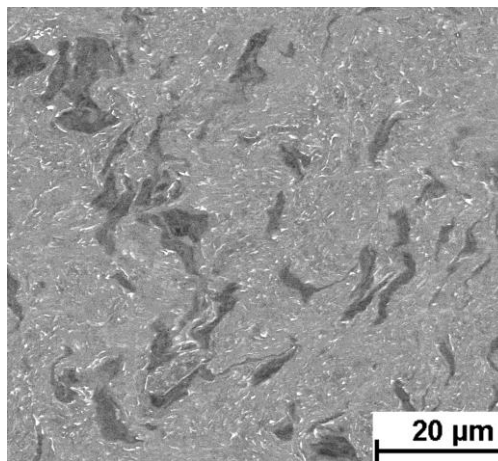Fig. 5.7 HPT deformed material (N = 5), center of the sample

Fig. 5.8 HPT deformed material (N = 5), 5 mm from the center of the sample
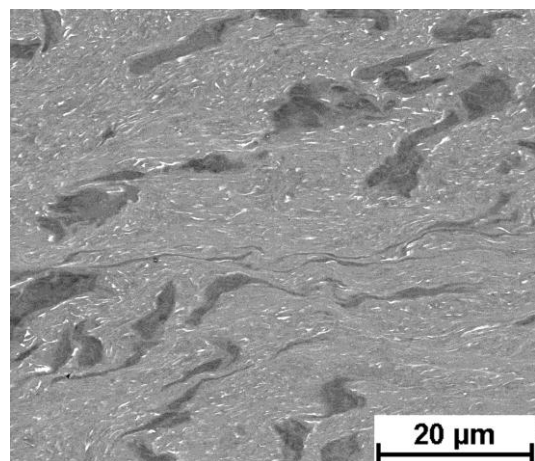
Fig. 5.9 HPT deformed material (N=5), edge of the sample

In the Fig. 5.8 is depicted the microstructure of the region that is 5 mm from the center of the sample after 5 HPT turns. Alpha grains are still visible, their shape is elongated and they are strongly deformed. Lamellar part is also deformed.

The microstructure of the zone near the edge of the specimen after 5 turns is shown in Fig. 5.9. The structure is more deformed and in the picture is observable the direction of the rotation during the deformation (left to right). However, original alpha grains are still recognizable.

The fragmentation of the primary α phase during deformation does not occur. This means, that the area of the alpha grains is the same even after 5 turns, only the shape of these grains have changed.
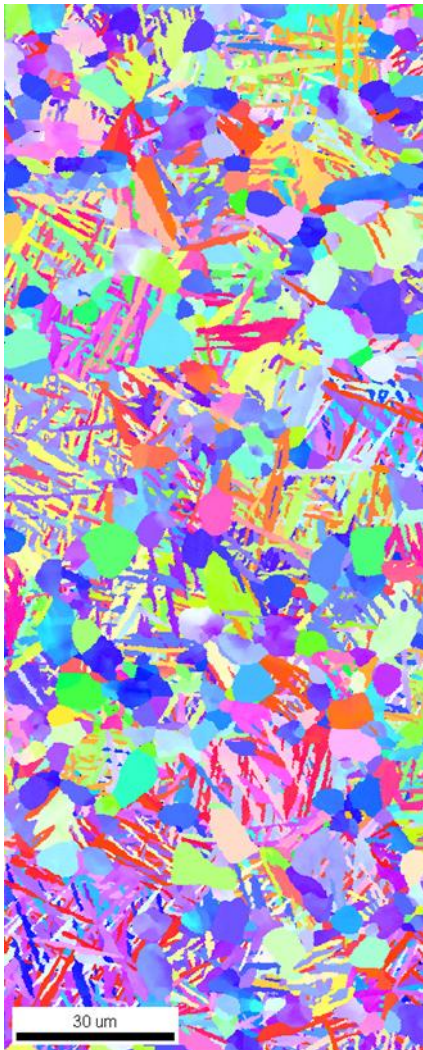
5.3 EBSD – Orientation Imaging

Fig. 5.10 shows inverse pole figure map of Ti-6Al-7Nb alloy in as-received (as-rolled) condition.

Bi-modal character of the Ti-6Al-7Nb alloy is clearly visible from the EBSD image. This type of structure contains equiaxed alpha grains and alpha lamellae in the alpha + beta regions. However, in the Fig. 5.10 only hcp alpha phase can be observed.

In the image, each point is coloured according to the crystallographic orientation. Relation between colouring and the orientation is given by orientation triangle shown in the Fig. 5.11.

Fig. 5.10 Inverse pole map figure of Ti-6Al-7Nb in as-rolled condition
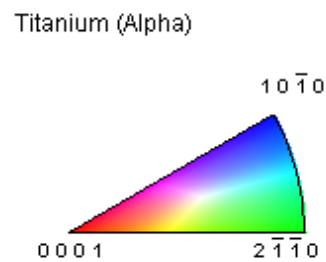
Fig 5.11 Orientation triangle

It can be seen that in the most of equiaxed primary alpha grains have constant orientation within the grain (the colour is homogeneous), but there are also cases when the colour of the grains is not homogeneous inside the grain. The reason is that the grain may be deformed and thus orientation relative to the other part of the grain is a little bit different.

On the other hand, it can be noticed that groups of alpha lamellae that are close to each and with the same spatial orientation have the same crystallographic orientation. It is caused by cooling from temperatures above beta transus temperature that forms alpha lamellae. This is described below in more detail.

EBSD images from material after HPT are not available due to ultra-fine and heavily deformed microstructure.

5.4 EBSD – Misorientation

Misorientation is the difference in crystallographic orientation between two grains in a polycrystalline material. Using electron back-scattered diffraction the grain misorientation in Ti-6Al-7Nb alloy can be characterized and the distribution of grain misorientations can be constructed. This histogram is shown in Fig. 5. 12. The picture shows also the theoretical (so-called Mackenzie) distribution [38]. Mackenzie distribution is theoretical distribution of misorientations when all grains are randomly oriented. Note that distribution in Fig. 5.12 significantly deviates from random distribution showing several peaks with preferred orientation.
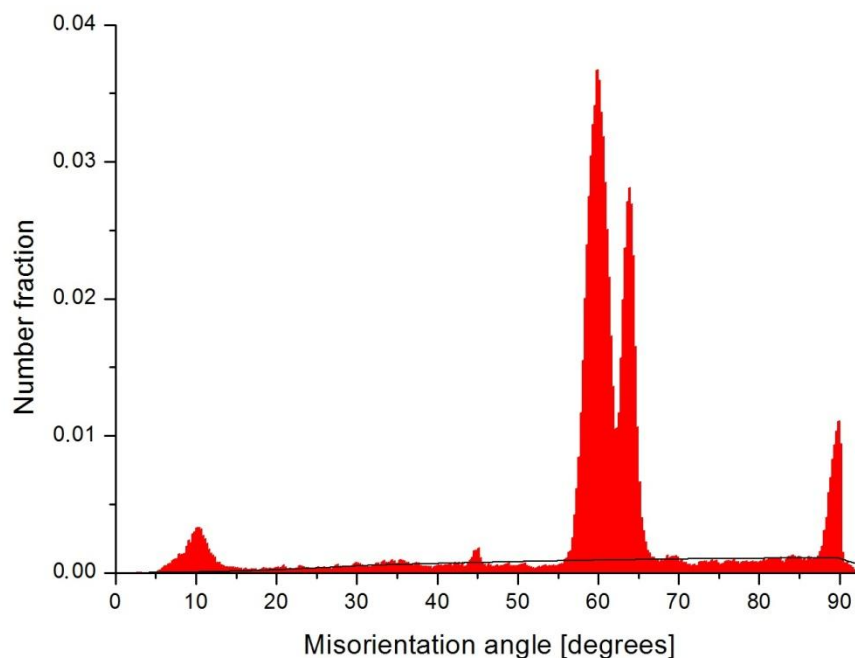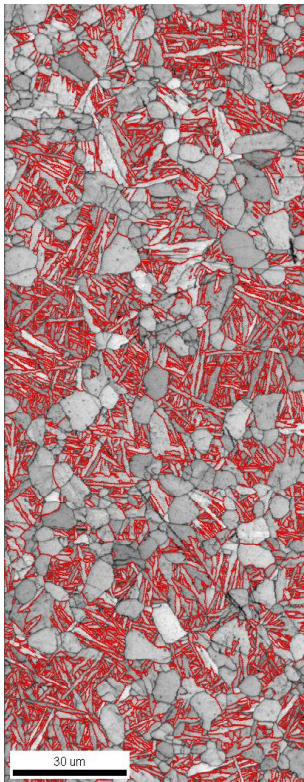

Fig. 5.12 Distribution of grain misorientation and the Mackenzie distribution

23

It has been described in the section Experimental material that upon cooling of Ti-6Al-7Nb alloy, alpha lamellae are created from beta grains. Alpha and beta phases are related by the Burgers orientation relation $(110)_\beta \| (00.2)_\alpha$ and $[-11-1]_\beta \| [2-1.0]_\alpha$ [37].

According to the Burgers relationship and the symmetry of α and β phases, a total of 12 different α orientations (12 variants) may arise from an initial β orientation during the β→α transformation. Theoretical misorientations between variants can be computed. Those are: of 60°; 60.83°; 63.26°; 90°; 10°. Furthermore, for random variant selection, the expected ratio of misorientations listed above can be computed and it is 2:3:2:2:1. [39].

However, apart of lamellae, equiaxed primary alpha grains are present in microstructure. The orientations of those grains have no special relation to their neighbours. Orientation of primary alpha grains is therefore assumed to be random and misorientations related to alpha primary grains obey the random (Mackenzie) distribution. As a result, measured distribution is a sum of random Mackenzie distribution due to primary alpha grains and peaks corresponding to selected misorientations between alpha lamellae.

In Fig. 5.13 grain boundaries with misorientations in the range of 55 – 65° are highlighted. It is clearly visible that such grain boundaries are preferably between two alpha lamellae.

On the basis of the histogram distribution of angles (Fig. 5.12) the ratio between peaks can be determined. In the Fig. 5.14 can be seen that the peaks for angles of 60° and 63.26° can be distinguished. In results from literature, these peaks are not distinguishable [40, 41]. On the other hand, peaks for angles of 60° and 60.83° cannot be distinguished from the histogram. The difference calculations and the calculations by Randle and Gey [40, 41] is that we subtracted a random distribution of orientation (Mackenzie distribution) because we used bimodal material. Afterwards, ration between peaks can be computed.

Fig. 5.13 Highlighted grain boundaries with misorientations in the range of 55°-65°
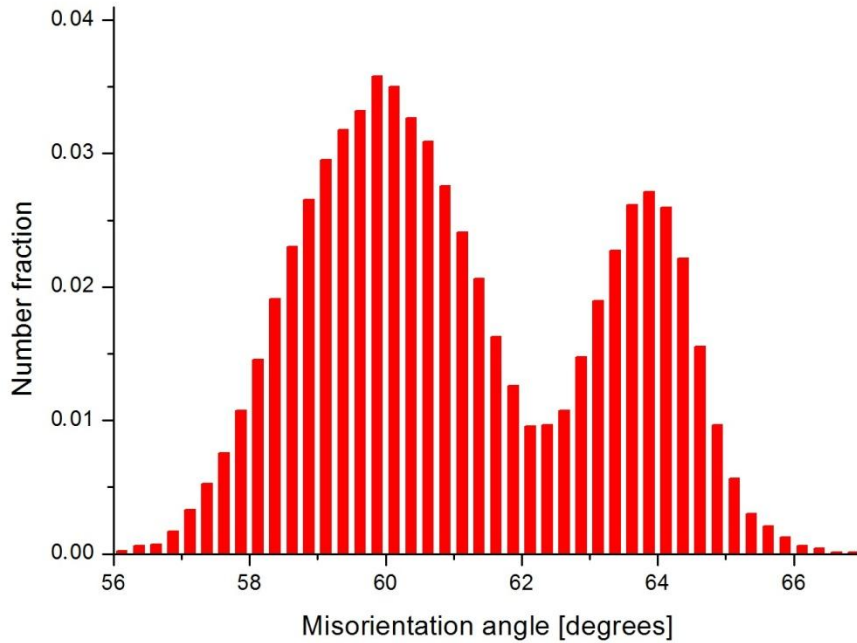
Fig. 5.14 Distribution of grain misorientations around 60°

Since peaks at 60° and 60.83° are not distinguishable, we can consider theoretical ratio as 5:2:2:1 for orientations 60° and 60.83°; 63.26°; 90°; 10°. According to our calculations the approximate ratio is 10:5:1:1. These results suggest that the variants of alpha lamellae are not chosen randomly, which is in accordance with results in literature. Non-random variants selection is not yet fully understood and will be further investigated.

5.5 Resistivity measurement of material after ECAP

Dependence of the electrical resistance on the temperature was measured in-situ during heating and cooling. Measurement was carried out in-situ in the non-commercial programmable furnace. The experimental arrangement is described in section 3.2.3. Electric current was supplied from a current source Keithley 2420 DC and resistivity of the sample was measured on Keithley 2182 nanovoltmeter. The Fig. 5.14 and 5.15 illustrate the prepared sample for the resistivity measurement.
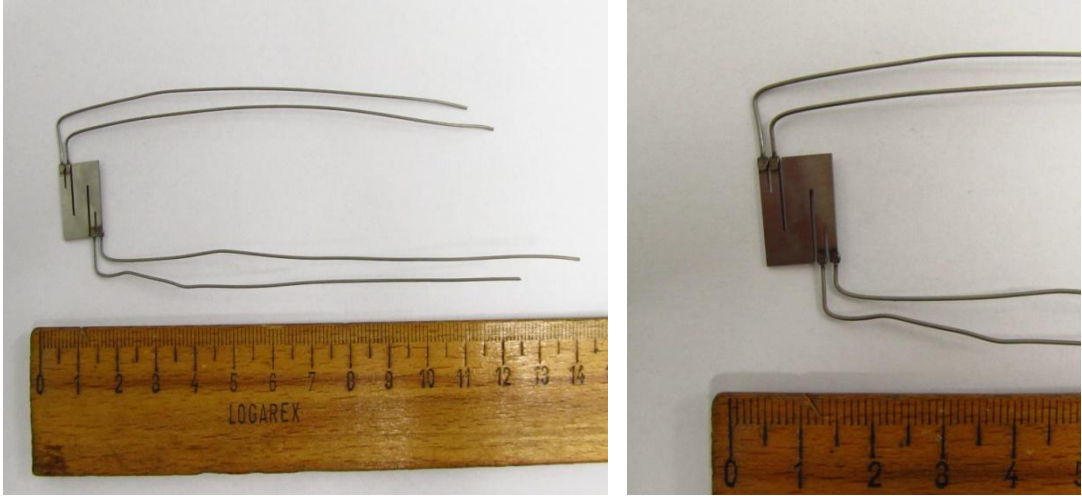
Fig 5.14 and Fig 5.15 Sample before resistivity measurement

In our case, measurement took place in three runs. Every run contains heating from room temperature up to 800 °C and cooling back to room temperature. The heating rate was 5 °C/min. Cooling rate was also set to 5 °C/min, but the furnace is not equipped with active cooling system and therefore the rate was maintained only down to approx. 400 °C, subsequent cooling was slower. Absolute resistivity of the sample is measured, however for the investigation of the dependence of resistivity on temperature the relative resistivity was computed by the formula:

$$Relative\ resisitivity = \frac{\rho_T - \rho_{50°C}}{\rho_{50°C}} \qquad (5.1)$$

Fig. 5.16 shows the dependence of the relative resistivity on the temperature during heating, Fig. 5.17 the dependence on the temperature during cooling.

According to the textbooks, resistivity grows linearly with the temperature obeying the Ohm's law. However, in our case, resistivity evolution for all three runs deviates significantly from the linear trend and, moreover, resistivity even decreases with increasing temperature above 650 °C. One of the reasons is that volume fraction of beta phase increases with rising temperature and beta phase is known to have lower resistivity [42].
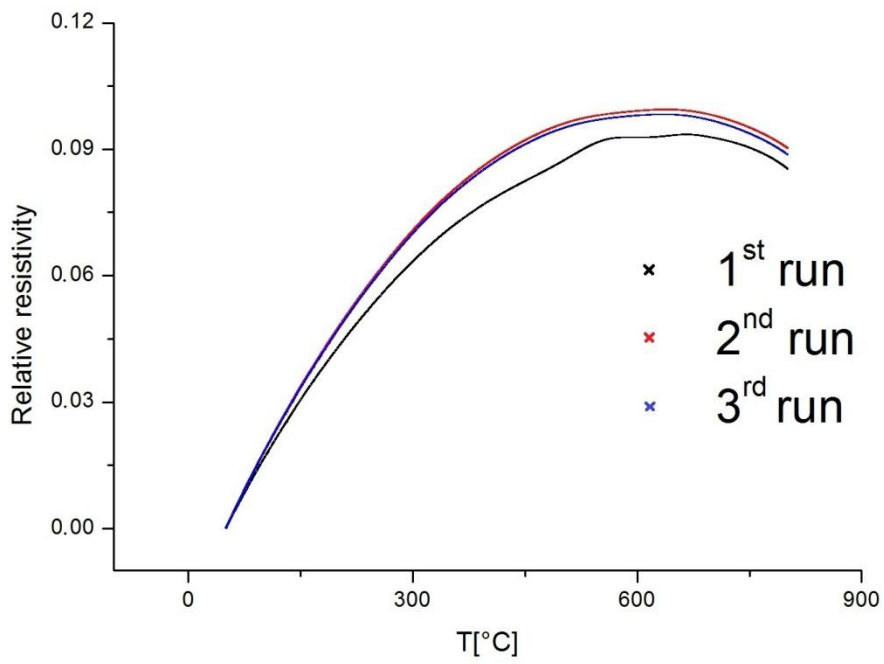
26

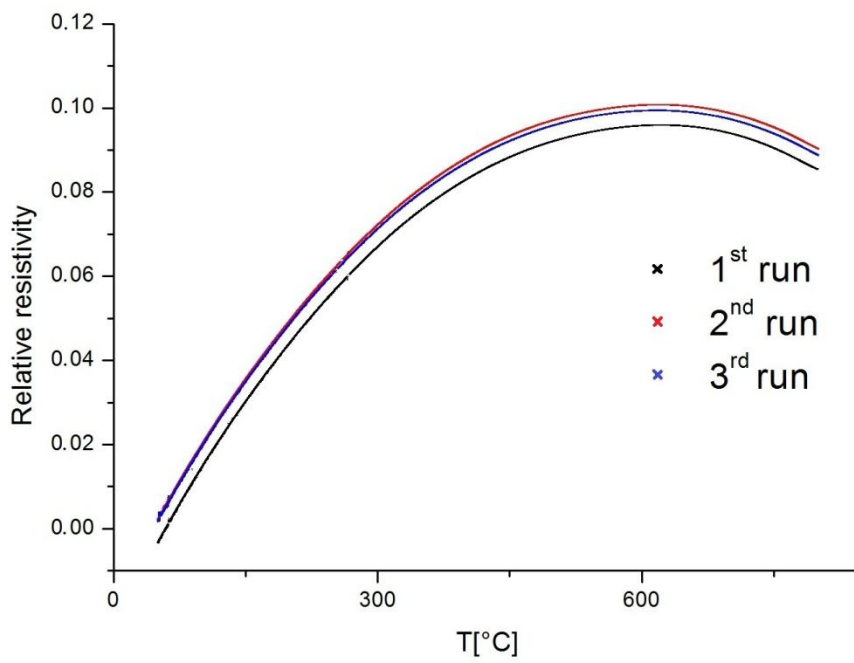Fig. 5.16 Dependence of the relative resistivity on the temperature during heating

Fig. 5.17 Dependence of the relative resistivity on the temperature during cooling

From the Fig. 5.16 it can be seen that there are obvious differences between heating in the first run in the area of higher temperature. The second and third run is similar to each other.

For heating first derivative is illustrated on the Fig. 5.18 to magnify differences between runs. Note that the first run has two peaks around 500 °C and 650 °C.
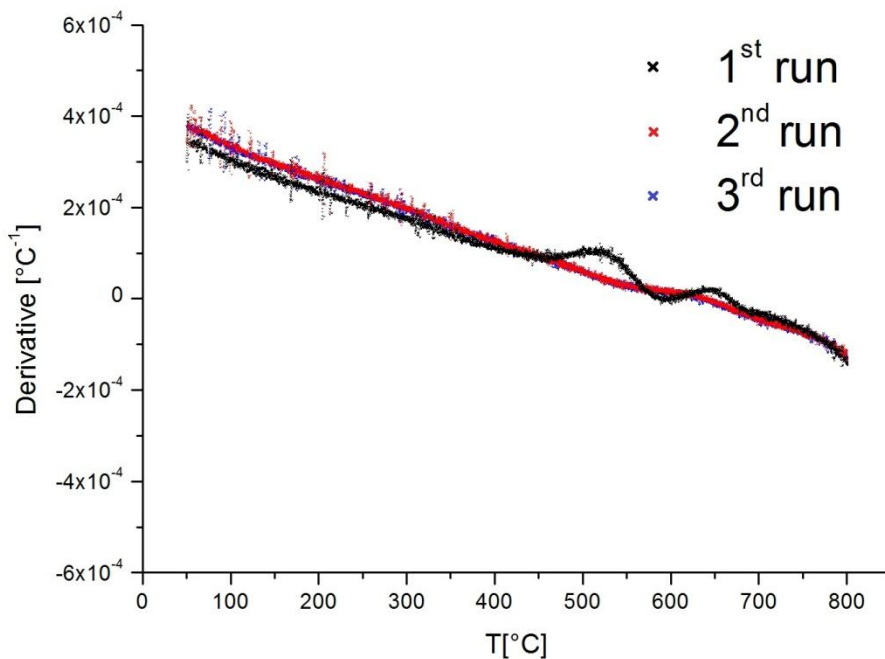
Fig. 5.18 First derivative of the relative resistivity depend on the temperature during heating

Processes that occur during the first heating are irreversible (since they are not repeated in the second and the third run) and are associated with original ultra-fine grained structure. This deformed structure is characterized by high density of dislocations and small grains. Both dislocations and grain boundaries may affect resistivity. It is therefore suggested that two measured differences in the first run are consequently associated with material recovery and recrystallization. The reason is that final temperature is below beta transus but assumed to be above recrystallization temperature.

Further structural measurements are necessary to prove this hypothesis.

6. Conclusions

In the present work titanium alloy Ti-6Al-7Nb and its properties were investigated. Ti-6Al-7Nb after high-pressure torsion was studied by microhardness measurements and SEM observations. Material after ECAP was used for electrical resistivity measurement. The most important results obtained by this investigation can be summarized as follows:

- Microhardness increases with increasing number of revolutions during HPT. However, significant increase in microhardness with the distance from the center of the specimen was not detectable. We found that the microhardness of samples after HPT is excessively heterogeneous. One of the reasons could be the bimodal structure of the alloy.

- Observations by scanning electron microscopy certify the bimodal structure. Two types of contrast are considered – Z-contrast and channeling contrast. Z-contrast shows different chemical composition of primary alpha grains interior when compared to alpha + beta regions. This result was confirmed by EDX measurements. The images of the sample after HPT show that the specimen is deformed, but the fragmentation of primary alpha grains does not occur. Observed deformation increases with the distance from the center of the sample.

- Misorientation between lamellae in alpha + beta region and also between lamellae and primary alpha grains was determined by electron back-scattered diffraction. We measured that the misorientation between alpha lamellae is not random and corresponds to Burger relationship describing beta →alpha transformation during thermal treatment. The ratio between the most probable angles of misorientation was computed: 60° and 60.83° : 63.26° : 90° : 10° = 10:5:1:1, which suggests that variants of alpha lamellae orientation are not chosen randomly.

- Measurement of resistivity evolution with the temperature exhibits a presence of irreversible process(es) during the heating. The irreversible process(es) appear(s) during the first heating as peaks in resistivity. The first peak may indicate material recovery and the second peak subsequent recrystallization.

29

Future work

Result of the present work shows interesting properties of the ultra-fine grained alloy Ti-6Al-7Nb after HPT and ECAP which requires further detail experimental analysis.

The further work will focus on the explanation of microhardness heterogeneity and explanation of resistivity data by microstructure observation and dislocation density measurement. The microstructure of the Ti-6Al-7Nb alloy will be investigated in more detail by transmission electron microscopy.

Bibliography

[1] G. Lütjering and J.C. Williams: Titanium, Springer Verlag, 2007, p.2.

[2] C. Leyens and M. Peters: Titanium and titanium alloys, Wiley-VCH, 2003, p.2.

[3] K. Katti: Biomaterials in total joint replacement, Col. and Surf. B: Biomat, 2004, vol. 39, p.133-142.

[4] M. Niinomi: Mechanical biocompatibilities of titanium alloys for biomedical applications, J. Mech. Behav. Biomed. Mat., 2008, vol. 1, p. 30-42.

[5] Wikipedia, Titanium alloy - Wikipedia, the free encyclopedia, 2013. [Online; Accessed 15-March-2013].

[6] E. O. Hall: The deformation and ageing of mild steel, Proc. Roy. Soc. B 64, 1951, p.747.

[7] N. J. Petch: The cleavage strength of polycrystalls, J. Iron Steel Inst. 174, 1953, p.25.

[8] U. Erb, A. M. El-Sherik, G. Palumbo, K. T. Aust: Synthesis, structure and properties of electroplated nanocrystalline materials, Nanostruct. Mater. 2, 1993, p. 383.

[9] R. Birringer, H. Gleiter, H. P. Klein: Nanocrystalline materials - an approach to a novel solid structure with gas-like disorder?, Phys. Lett. A 102, 1984, p. 365.

[10] J. S. Benjamin: Dispersion strengthened superalloys by mechanical alloying, Metall. Trans. 1, 1970, p. 2943.

[11] D. B. Witkin, E. J. Lavernia: Synthesis and mechanical behavior of nanostructured materials via cryomilling, Prog. Mater. Sci. 51, Volume 51, Issue 1, 2006, p. 1–60.

[12] V. M. Segal, V. I. Reznikov, A. E. Drobyshevskiy, V. I. Kopylov: Plastic working of metals by simple shears, Russian Metall, 1981, p. 99-105.

[13] R. I. Kuznetsov, V. I. Bykov, V. P. Chernyshev, V. P. Pilyugin, N. A. Yefremov, A. V. Pasheyev: Plastic deformation of solid bodies under pressure-1: Equipment and methods. Preprint 4/85, IFM UNTs AN SSSR, Sverdovsk, USSR, 1985.

[14] N. A. Smirnova, V. I. Levit, V. I. Pilyugin, R. I. Kuznetsov, L. S. Davydova, V.A. Sazonova: Evolution of the structure of f.c.c. single crystal subjected to strong plastic deformation, Fiz. Metal. Metalloved 61 (6) (1986), p. 1170.

[15] Y. Saito, H. Utsunomiya, N. Tsuji, T. Sakai: Novel ultra-high straining process for bulk materials - development of the accumulative roll-bonding (ARB) process, Acta Mater. 47, 1999, p. 579.

[16] W. M. Thomas, E. D. Nicholas, J. C. Needham, M. G. Murch, P. Temple-Smith, C. J. Dawes: GB Patent No. 9125978.8 (1991), US Patent No. 5460317, 1995.

[17] R. S. Mishra, M. W. Mahoney, S. X. McFadden, N. A. Mara, A. K. Mukherjee: High strain rate superplasticity in a friction stir processed 7075 Al alloy, Scripta Mater. 42, 2000, p. 163.

[18] Y. T. Zhu, H. Jiang, J. Huang, T. C. Lowe: Method for producing ultrafine-grained materials using repetitive corrugation and straightening, Metall. Mater. Trans A 32, 2001, p. 1559.

[19] Y. T. Zhu, T. C. Lowe, H. Jiang, J. Huang: US Patent No. 6197129, 2001.

[20] Y. Beygelzimer, V. Varyukhin, D. Orlov, S. Synkov, A. Spuskanyuk, Y. Pashinska. In: M. J. Zehetbauer, R. Z. Valiev, editors: Nanomaterials by severe plastic deformation. Weinheim, Germany: Wiley-VCH Verlag, 2004, p. 511.

[21] V. N. Varyutkhin, Y. Beygelzimer, S. Synkov, D. Orlov: Application of Twist Extrusion, Mater Sci Forum 503-504, 2006, p. 335.

[22] Y. Iwahashi, J. Wang, Z. Horita, M. Nemoto, T. G. Langdon: Principle of equal channel angular pressing for the processing of ultra-fine grained materials, *Scripta Mater.*, 1996, 35, p. 143.

[23] J. Vrátná, M. Janeček, J. Čížek, Dong Jun Lee, Eun Yoo Yoon, Hyoung Seop Kim: "Mechanical properties and microstructure evolution in ultrafine-grained AZ31 alloy processed by severe plastic deformation", Journal of Materials Science, 2013, Volume 48, Issue 13, pp 4705-4712.

[24] M. V. Degtyarev, T. I. Chashchukhina, L. M. Voronova, A. M. Patselov, V. P. Pilyugin: Influence of the relaxation processes on the structure formation in pure metals and alloys under high-pressure torsion, Acta Mater. 55, 2007, p. 6039.

[25] A. P. Zhilyaev, G. V. Nurislamova, B. K. Kim, M. D. Baro, J. A. Szpunar, T. G. Langdon: Experimental parameters influencing grain refinement and microstructural evolution during high-pressure torsion, Acta Mater. 51, 2003, p. 753.

[26] A.P. Zhilyaev, K. Oh-ishi, T.G. Langdon, T.R. McNelley: Texture and microstructural evolution in pure aluminum during high-pressure torion, Mater, Sci Eng A 410-411, 2005, p. 277.

[27] Y. Harai, Y. Ito, Z. Horita: High-pressure torsion using ring specimens Original Research Article, Scripta Materiala, Volume 58, Issue 6, March 2008, p. 469-472.

[28] V.Polyakova, I. Semenova, R. Valiev: Influence of annealing on the structure and mechanical properties of ultrafine-grained alloy Ti-6Al-7Nb, processed by severe plastic deformation, Materials Science Forum 667-669, 2010, p. 943.

[29] G. Lütjering and J.C. Williams: Titanium. Springer Verlag, 2007, p.208.

[30] Miloš Janeček, Josef Stráský, Jakub Čížek, Petr Harcuba, Kristína Václavová, Veronika V. Polyakova, Irina P. Semenova - Mechanical properties and dislocation structure evolution in Ti-6Al-7Nb alloy processed by high pressure torsion, 2013.

[31] Veronika Polyakova, Irina P. Semenova, Ruslan Valiev - Influence of annealing on the structure and mechanical properties of ultrafine-grained alloy Ti-6Al-7Nb, Processed by severe plastic deformation, Materials Science Forum, volumes 667 - 669, 2010, p. 943-948.

[32]Jana Šmilauerová, Phase transformations and microstructure changes in TIMET LCB alloy, Master thesis, Charles University in Prague, 2012, p. 17.

[33] J. I. Goldstein, D. E. Newbury, P. Echlin, D. C. Joy, C. E. Lyman, and E. Lifshin: Scanning electron microscopy and X-ray microanalysis, Kluwer Academic/Plenum Publish, 2003.

[34] Wikipedia, Energy-dispersive X-ray spectroscopy – Wikipedia, the free encyclopedia, 2013. [Online; accessed 26-February-2013].

[35] E. W. Collings. The physical metallurgy of titanium alloys, American Society for Metals, 1984.

[36] Jitka Vrátná, Miloš Janeček, Jakub Čížek, Dong Jun Lee, Eun Yoo Yoon, Hyoung Seop Kim: "Mechanical properties and microstructure evolution in ultrafine-grained AZ31 alloy processed by severe plastic deformation", Journal of Materials Science, 2013, Volume 48, Issue 13, p. 4705-4712.

[37] Y. Estrin, M. Jane_ek, G.I. Raab, R.Z. Valiev and A. Zi: Severe plastic deformation as a means of producing ultra-fine grained net-shaped micro electro-mechanical systems parts, Metall. Mater. Trans. A, 2007, vol. 38, p. 1906-1909.

[38] J. K. Mackenzie: The distribution of rotation axes in a random aggregate of cubic crystals Acta Metallurgica, Volume 12, Issue 2, February 1964, p. 223-225

[39] G. Lütjering and J.C. Williams: Titanium. Springer Verlag, 2007, p.210.

[40] V. Randle,a, G.S. Rohrerb and Y. Hua: Five-parameter grain boundary analysis of a titanium alloy before and after low-temperature annealing, Scripta Materiala, 2007, p.184.

[41] N. Gey, M. Humbert: Characterization of the variant selection occurring during the α→β→α phase transformations of a cold rolled titanium sheet, Acta Materiala, 2001.

[42] Jana Šmilauerová, Phase transformations and microstructure changes in TIMET LCB alloy, Master thesis, Charles University in Prague, 2012, p. 29.